Discrimination of Photon- and Dark-Initiated Signals in Multiple Gain Stage APD Photoreceivers

George M. Williams, David A. Ramirez, Majeed Hayat, and Andrew S. Huntington

***Abstract*—We demonstrate the ability of linear mode single carrier multiplication (SCM) avalanche photodiode (APD) -based optical receivers to discriminate single-photon-initiated avalanche events from dark-current-initiated events. Because of their random spatial origin in discrete regions of the depletion region, in the SCM APD the dark-generated carriers multiply differently than the photon-generated carriers. This causes different count distributions and necessitates different statistical descriptions of the signal contributions from photon- and dark-originating impulse responses. To include dark carriers in the performance models of the SCM APD, we considered the influence of the spatial origin of the ionization chains on a receiver's noise performance over the times the optical pulse is integrated by the receiver's decision circuits. We compare instantaneous (time-resolved) numeric and pseudo-DC analytical models to measured SCM APD data. It is shown that it is necessary to consider both the distribution of spatial origin and the instantaneous properties of the ionization chains to describe statistically an SCM APD receiver. The ability of SCM APD receivers to discriminate single photon events from single dark events is demonstrated, and the effective gain and excess noise contributions of the light- and dark-initiated avalanche events and their influence on receiver sensitivity and signal-to-noise characteristics are shown.**

***Index Terms*—APD, Avalanche Buildup, Avalanche Photodiode, Excess Noise, Numeric Modeling, Photoreceiver, SCM, Single Carrier Multiplication, Superlattice APD**

I. Introduction

AVALANCHE photodiodes (APDs) have been widely deployed in telecommunications and laser radar imaging systems. The popularity of APDs in high-speed photoreceivers is attributed to their ability to provide high internal optoelectronic gain, which allows the photogenerated electrical signal to dominate the thermal, or Johnson, noise in the preamplifier stage of the receiver module without the need for optical pre-amplification of the received optical signal [1]. The optoelectronic gain results from the cascade of electron and hole impact ionization that takes place in the high-field intrinsic multiplication layer of the APD [2]. Due to its stochastic nature, however, this avalanche multiplication process is inherently noisy, resulting in random fluctuations in the gain. Thus, the benefit of the gain is accompanied by a penalty; the shot noise present in the photon-generated electrical signal is accentuated according to the APD excess noise factor, which is a measure of the uncertainty associated with the stochastic nature of the APD gain [2]. Additionally, the increased electric field strength required for avalanche gain can increase APD dark current.

Most of the III–V semiconductor materials sensitive to the telecommunications wavelengths have comparable ionization rates for electrons and holes; thus, they are unsuitable for fabrication of low-noise APDs. This has led to consideration of artificially enhancing the electron-to-hole ionization ratio by using multilayer heterojunctions or superlattice structures [3]–[6]. To reduce the effects of excess noise on photoreceiver performance, we have developed a separate absorption, charge, and multiplication (SACM) single carrier multiplication (SCM) APD [7]–[9]. The SCM APD device shown in Fig. 1 consists of an InGaAs absorption layer, a charge layer, and a multiplication layer consisting of a cascade of quantity J discrete heterostructured InAlAs gain stages.

It is known that very low-noise avalanche gain is achieved in an APD if only electrons impact ionize, so that the feedback noise associated with two-carrier ionization is avoided, and the electron multiplication occurs with high probability at discrete locations of the multiplication region, so that the variability of the number of electrons generated per photon is minimized [10]. Accordingly, each of the SCM APD heterostructured gain stages is designed to locally enhance electron ionization and to suppress hole ionization.

In the SCM APD shown in Fig. 1, the photons absorbed in the absorption region generate a Poisson distributed primary photocurrent. The photoelectrons enter the multiplication region and drift in the positive x direction, toward the $n+$ cathode. In the high-field low-threshold regions of each of the J gain stages, the photoelectrons and their electron progeny ionize, with probability, P, whereby they generate electron-hole pairs. The hole carriers, drifting toward the $p+$ anode, pass through "cool down" layers situated between the gain stages such that individual hole carriers spend very little time with kinetic energy in excess of the ionization threshold; this suppresses the probability of hole ionization in each gain stage, U, so that low noise avalanche multiplication is achieved [9].

Fig. 2 shows a numeric model of the spatial occurrence of hole- and electron-initiated impact ionization events that

Manuscript received February 13, 2013; revised April 4, 2013 and April 11, 2013; accepted April 12, 2013. Date of publication May 15, 2013; date of current version August 19, 2013. The review of this paper was arranged by Prof. A.G. Unil Perera.

G. M. Williams and A. S. Huntington are with Voxtel, Inc., Beaverton, OR 97006 USA (e-mail: georgew@voxtel-inc.com; andrewh@voxtel-inc.com).

D. A. Ramirez and M. Hayat are with the Center for High Technology Materials, University of New Mexico, Albuquerque, NM 87106 USA (e-mail: dramirez@skinfrared.com; hayat@chtm.unm.edu).

Color versions of one or more of the figures in this paper are available online at http://ieeexplore.ieee.org.

Digital Object Identifier 10.1109/JEDS.2013.2263196

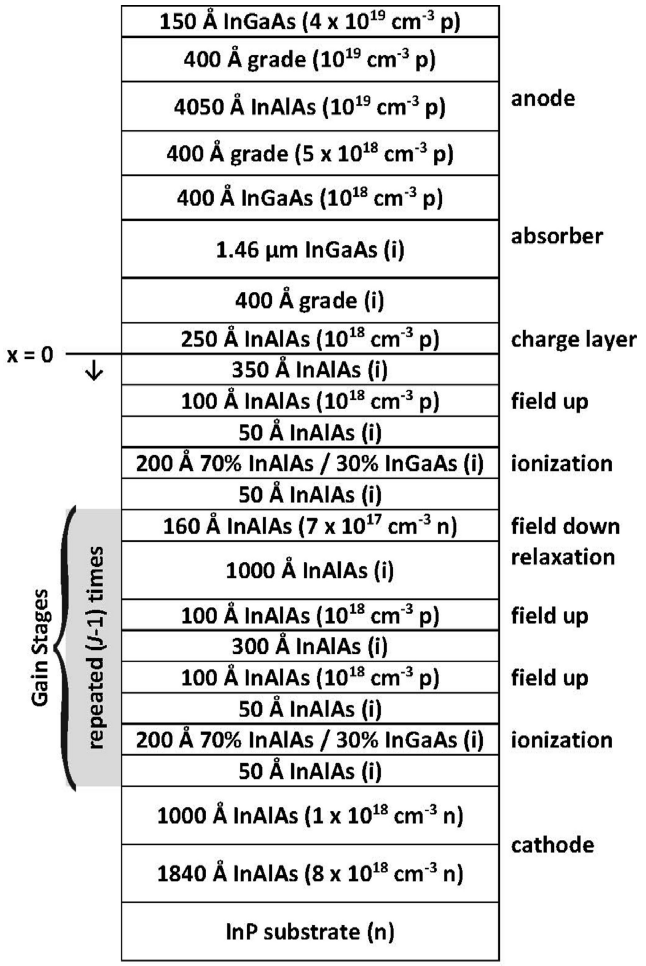

Fig. 1. Epitaxial layer structure of a (J) stage SCM APD.

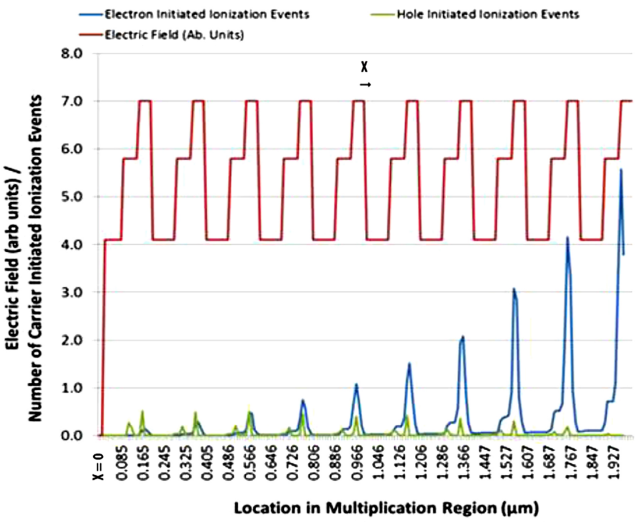

Fig. 2. The spatial location of hole- and electron-initiated impact ionization events generated by a numeric model of the carrier dynamics of a 10-stage SCM APD multiplication region. Each of the gain stages employs variations in alloy composition and doping, which creates the electric field profile onto which is superimposed the spatial count of ionization events.

occur in a 10-gain-stage SCM APD biased for an average DC gain of $M = 940$, which, at high gain, due to the ratio of electron ionization events to hole ionization events, has an excess noise characterized by the McIntyre-equation [11], when parameterized by $k = 0.02$. Also plotted is the normalized electric field profile modeled across the multiplication region, showing the ionization events to occur primarily in the high field regions of the gain stages.

Teich et al. [12] have found that the theory of discrete ionization processes proposed by Van Vliet and co-workers [13] for conventional short avalanche region APDs is applicable for cascaded discrete gain stage APDs assuming single ionization per stage. Measured SCM APD data is in better agreement with these models than the McIntyre-model [9]. However, these earlier works, describing the properties of multi-gain-stage devices, do not consider dark carrier generation, do not provide the photon- and dark-initiated avalanche count distributions, and do not describe the instantaneous temporal properties of the impulse response.

Such performance characteristics are important for considering APD photoreceiver performance. In an APD, the process of carrier multiplication, in addition to causing gain fluctuations, also introduces time response fluctuations, and the impulse response is best modeled as a stochastic process composed of the statistically correlated random variables of avalanche buildup time (pulse duration) and integrated signal (the multiplication factor). This is significant, as when modeling the detection of short optical pulses, instantaneous avalanche gain cannot be assumed, and the temporal dynamics of the photon- and dark-initiated carriers on the detection process must be considered [8].

It is the difference between the time-resolved probability density functions (PDFs) of the photon-initiated and dark-initiated avalanche event contributions to the impulse response that allow discrimination of photon-initiated from dark-initiated avalanche events in SCM-APD-enabled photoreceivers. This capability is not found in photoreceivers configured with common APD designs, wherein the multiplier's high field region is adjacent to the absorption layer, so that dark-initiated and photoelectron-initiated ionization events experience the same mean avalanche gain.

II. SCM APD Dark-carrier Generation

A. Discussion of Dark Current Generation in APDs

To determine the count distributions and low order statistics of the SCM APD's response to optical and dark originating ionization chains, we considered the influence of the spatial origin of the carrier ionization chain on the signal current present at the external decision circuits of a photoreceiver.

In avalanche detectors, dark counts arise primarily from the injection of charge carriers into the junction by three phenomena: 1) thermal excitation; 2) tunneling across the depletion region; and 3) emission by trapping centers [14], [15]. The thermal generation results from carriers transferred from the valence band to the conduction band either directly or via the midgap defects, owing to thermal excitation. The thermal generation and recombination (G–R) processes are described by the Shockley-Read-Hall (SRH) model [16]. The

thermal generation rate per unit volume N_{th} can be expressed as

$$N_{th} = \frac{n_i}{\tau_{SRH}} \quad (1)$$

where n_i is the intrinsic carrier concentration and τ_{SRH} is the lifetime related to the SRH processes. In practice, the temperature dependence of G–R current in an SACM APD may be observed to come primarily from the intrinsic carrier concentration of its absorber [17]

$$n_{i,abs}(T) = 2\times\left[\frac{2\pi k_B T}{h^2}\right]^{\frac{3}{2}}\times\left[m_e^* m_h^*\right]^{\frac{3}{4}}\times\exp\left[-\frac{E_g(T)\,q}{2\pi k_B T}\right], \quad (2)$$

where h is Planck's constant, q is the charge on an electron, k_B is Boltzmann's constant, m_e^* and m_h^* are carrier effective masses (the density of states values), and $E_g(T)$ is the temperature-dependent band gap. The temperature-dependent band gap (in eV) of $Al_yGa_xIn_{1-x-y}As$ is modeled by [18]

$$E_g\left(Al_yGa_xIn_{1-x-y}As, T\right) = 0.360 + 0.629x + 2.093y + 0.436x^2 + 0.577y^2 + 1.013xy - 4.1\times10^{-4}\left[\frac{T^2}{T+136} - \frac{300^2}{300+136}\right]. \quad (3)$$

The trap-assisted tunneling (TAT) mechanism of electron- and hole-transfer from the conduction band to the valence band and vice versa, is described by exchange processes represented by their tunneling escape times. Generation by TAT is generally a two-step process. In the first step, an electron is promoted out of the valence band and into a mid-gap trap state. This generates a mobile hole in the valence band and an occupied trap. The second step occurs if the trapped electron manages to tunnel from the trap state into the conduction band before it recombines with a hole in the valence band. Tunneling completes the generation of a new electron-hole pair, whereas recombination resets the system to its original state.

The complex TAT process depends on the trap position inside the energy gap, the trap density, the trap occupation by electrons, and the height and width of the trap potentials (the amount that the tunneling energy or barrier height is reduced from E_g). As a result, TAT-generated dark currents have a strong dependence on the bias-dependent electric field [19].

Dark carrier generation by band-to-band tunneling (BBT) is very similar to the second step of trap-assisted tunneling. Two important differences are: 1) the density of states involved—the density of states at the valence band edge greatly exceeds the possible density of trap states; and 2) the height of the potential barrier—the full band gap. Consequently, BBT rates are significant in narrow-gap semiconductor alloys, which is why the SCM APD employs an SACM structure, wherein the narrow-bandgap absorption region is separated from the high field multiplication region by a charge layer.

An analytic expression for the BBT rate in direct gap semiconductors has been derived that depends upon the electric field strength, F, and the temperature-dependent band gap. The generation rate per unit volume can be expressed as [20]

$$N_{BBT}(T) = \frac{\sqrt{2m^*}q^3 FV}{\sqrt{E_g(T)}4\pi^3\hbar^2}\exp\left(-\frac{\pi\sigma_{(T)}(m^*)E_g^{3/2}(T)}{2\sqrt{2}q\hbar F}\right) \quad (4)$$

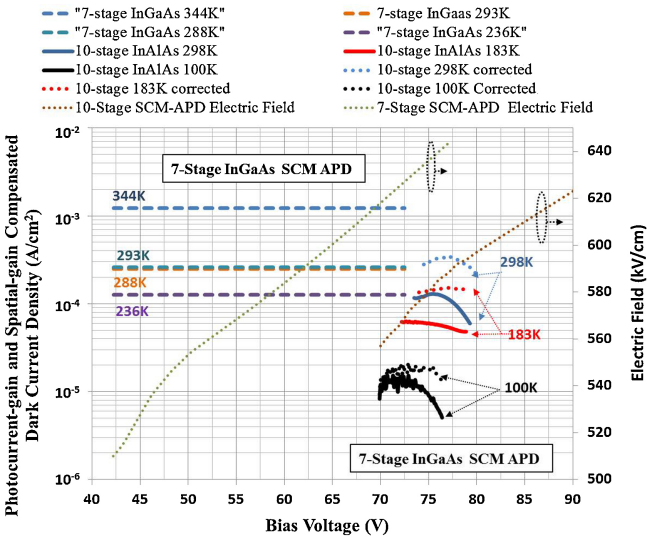

Fig. 3. Gain-normalized dark current measured for the 7-stage and 10-stage SCM APD at various temperatures. The gain is compensated for saturation effects and breakdown voltage shifts, but not the difference in output distributions between multiplied photoelectrons (originating at $x=0$) and dark carriers (distributed randomly in the gain stages). The dashed lines of the 10-stage data show the dark current data compensated for the dark carrier ionization chain's spatial origin.

where $\hbar$ is the reduced Planck's constant, the effective carrier mass for AlGaInAs is $m^* = 0.08m_o$, where $m_o = 9.11\text{x}10^{-31}$; and $\sigma(T) = 1.18$. In an operational fully depleted SACM APD, the electric field strength, F, is linear as a function of applied bias.

B. Measured SCM APD Dark Current

The photocurrent-gain normalized dark current data measured from 7-stage and 10-stage SCM APDs operated at various temperatures are shown in Fig. 3. Also shown are the estimated electric fields present in the multiplication region at each bias; these were estimated using a band edge modeler [21].

The SCM APDs tested were grown on InP substrates by molecular beam epitaxy (MBE) and are identical in design, with the exceptions that the number of gain stages differ and the 7-stage SCM APDs included an $Al_0Ga_{0.47}In_{0.53}As$ (InGaAs) absorption region with a room temperature bandgap energy of ~ 0.75 eV, optically active over the 950-nm to 1 500-nm spectral range; whereas the 10-stage SCM APDs were grown with an $Al_{0.072}Ga_{0.398}In_{0.530}As$ (InAlGaAs) absorption layer. The absorber's 0.86 eV bandgap allows it to be optically sensitive over the 950-nm to 1 500-nm spectral range [7]. In both the 7-stage and 10-stage SCM APDs, each of the multiplier gain stages includes an $Al_{0.335}Ga_{0.140}In_{0.525}As$ alloy layer (see Fig. 1), which from (3) has a bandgap of 1.27 eV. The ratio of the conduction band offsets to the valence band offset for $Al_{0.335}Ga_{0.140}In_{0.525}As$ to InGaAs is approximately 70:30.

The measurements were carried out by means of I–V curves and simultaneous measurements of average gain and noise power spectral intensity. The data were collected using a computer-controlled HP 4155A semiconductor parameter analyzer (SPA). The SPA applied the bias to the SCM APD mounted on a temperature-stabilized cold post located

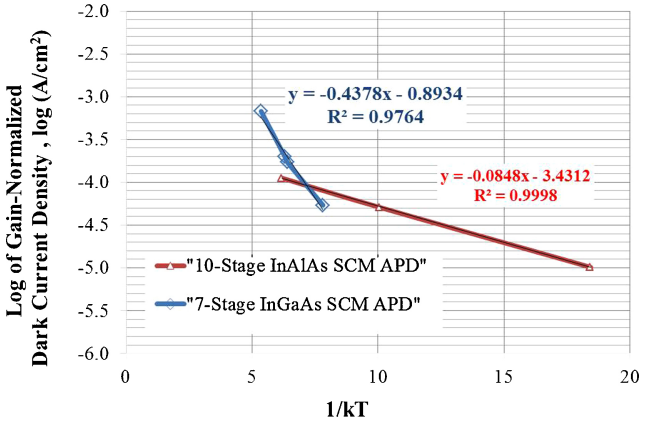

Fig. 4. Arrhenius plots of the Fig. 3 data for the 7-stage and 10-stage SCM APDs, including exponential curve fitted to the data.

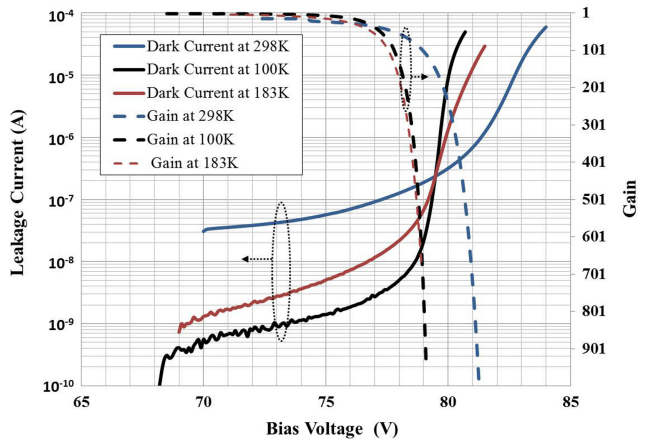

Fig. 5. Current vs. voltage (primary y axis) and gain vs. voltage (secondary y axis) curves for 10-stage SCM APDs measured at 298K, 187K, and 100K.

inside a windowed vacuum cryochamber. A 38 nW 1 064-nm wavelength optical signal was projected from an OZ Optics OZ-2000 stabilized fiber-coupled diode laser, through the window of the cryochamber, and onto a spot that underfilled the SCM APD optically active area. A bias tee coupled the DC component of the diode current to the SPA and sent the AC component to an HP 8447D high-speed pre-amplifier, which fed either an HP 8566B spectrum analyzer or an HP 8970B noise figure meter.

Gains were calculated using multiple light levels so that high signal-to-noise measurements could be obtained over the range of biases, allowing saturation effects to be compensated.

The temperature-dependent photocurrent-gain-normalized dark current data in Fig. 3 show a 2.92 mV/K breakdown voltage shift for the 7-stage SCM APDs grown with the InGaAs absorber. The measured dark current levels show little electric field dependence. For the 7-stage devices, the photocurrent-gain-compensated data values at each temperature are largely independent of operating bias, implying dark current dominated by thermal generation of carriers in the absorption region. The Arrhenius plot of Fig. 4, within the error limits of the three-point curve fit, shows an activation-energy slightly greater than the $\sim$ 0.75 eV bandgap of the InGaAs absorber. Further fitting of the extracted data from the temperature measurements, performed using a thermal emission current model (2), confirmed that the APD dark current is dominated by thermal generation in the InGaAs absorber. In this case, the dark-generated carriers traverse all gain stages and experience the same net gain as the photon-generated carriers.

Unlike the 7-stage InGaAs absorption region SCM APD data, the photocurrent-gain-compensated dark current data from the 10-stage InAlGaAs absorption region devices show a bias dependence. The electric field dependence of the data suggests that the dark carriers in the 10-stage SCM APDs are primarily generated via tunneling mechanisms, such as might be described by (4). In the SCM APD, tunneling currents may originate either in the absorption region or in the thin AlGaInAs high field regions of the multiplier. The bias dependence of the photocurrent-gain-normalized data suggests the latter.

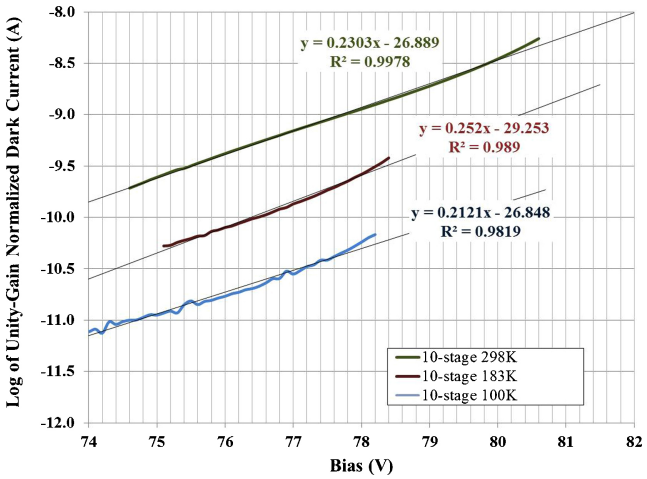

Fig. 6. Log plots of the measured unity-gain-normalized tunneling dark current versus voltage for the 10-stage SCM APD.

The I–V and gain curves for the 10-stage InAlGaAs APD at 298K, 187K, and 100K are shown in Fig. 5. The data show a 3.65 mV/K breakdown voltage shift as a function of temperature. The breakdown voltage shift is a result of increased phonon vibrations at elevated temperatures, which decreases carrier mean free-paths and causes the ionization probabilities, and resultant multiplication gains, to decrease.

The logarithms of the measured unity-gain-normalized dark current densities shown in Fig. 6 are linearly proportional to the inverse temperature and are proportional to the inverse bias. From (4), the extracted average activation energy of traps is approximately $\sim$ 0.45 eV. This is within the published 0.45 to 0.75 eV range of deep level traps observed in InAlAs [22], [23]. In this case, conduction occurs primarily in the conduction band itself, and the activation energy is given by deep level emission.

We assumed the traps to originate from oxygen incorporation into the InAlAs materials during the MBE process [24]. Due to the chemical affinity of oxygen for aluminum, oxygen contamination is a major source of mid-gap traps in III–V compound semiconductors. Oxygen traps can be a couple

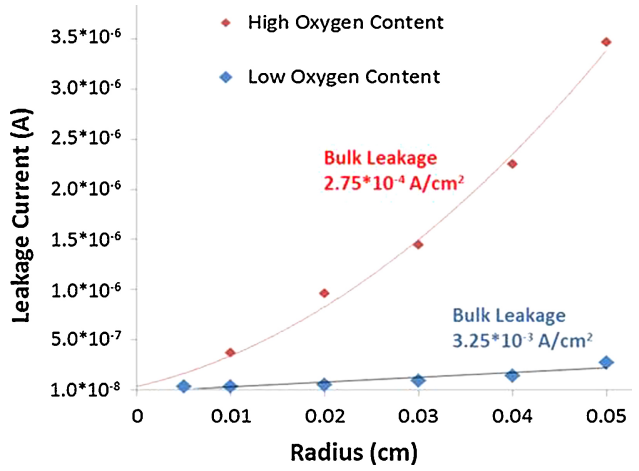

Fig. 7. Measure of dark current as a function of device diameter showing the effects of oxygen on dark current.

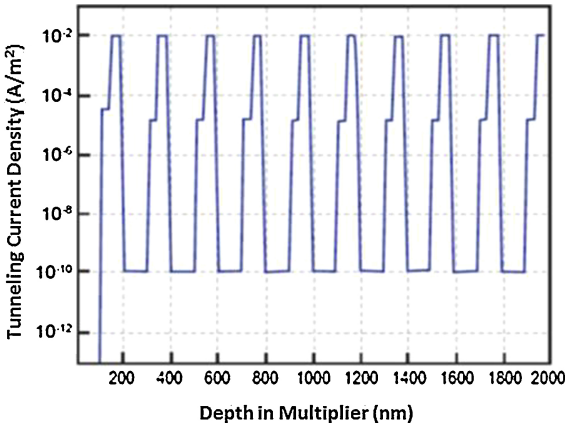

Fig. 8. SCM APD dark current generation rate modeled from (4) using electric field of Fig. 2 showing generation as a function of location in the multiplication layer ($x = 0$ is the location of photoelectron injection).

orders of magnitude greater in density of aluminum-containing alloys than in aluminum-free alloys.

To confirm this hypothesis, and to quantify the sensitivity of the SCM APD devices to oxygen-induced defects, a series of 1-μm thick InAlAs multiplication region InGaAs/InAlAs APDs were grown at temperatures ranging from 700°C to 720°C. Changes in oxygen content were achieved by adjusting the wafer growth conditions—Fairly small changes in substrate temperature and the supply of reactants can have a large impact on the incorporation rate of oxygen impurities. SIMS was used to measure oxygen concentration ranging from roughly 10^{18} cm^{-3} to 10^{17} cm^{-3}.

Fig. 7 shows the measured dark current from APDs of varying diameters manufactured under different growth conditions. The APD dark current can be divided into two categories by the leakage path: 1) the bulk leakage current, which is proportional to the mesa area; and 2) the sidewall leakage current, which is only proportional to the mesa perimeter. The measured dark currents were fitted to the mesa diameter using a quadratic fit at a bias voltage of approximately 90 percent of the breakdown voltage. An almost perfect quadratic fit was achieved; thus, the bulk leakage current was found to be dominant for large area devices. The drop in bulk dark current density for the decade change in oxygen concentration was nearly an order of magnitude—from 275 μA/cm^2 to 32.5 μA/cm^2.

The dark current data support the notion that the 10-stage SCM APD dark currents were dominated by oxygen-induced TAT processes. However, whereas (4) predicts dark current to increase as a function of bias, the data in Fig. 3 show a decrease in gain-normalized dark current as a function of applied electric field. Significantly, the dark current data of Fig. 3 were compensated for the photocurrent-gain values of Fig. 5, which assumes that the dark carriers experience the full gain of the multiplier. However, a characteristic of the SCM APD is that dark carriers may originate in the high field region of any of the discrete gain stages, and are unlikely to experience the same mean gain experienced by photoelectrons.

Fig. 8 illustrates the spatially resolved dark current generation rate data of a 10-stage SCM APD modeled using (4) and the electric field profile of Fig. 2. The modeled data is consistent with the measured SCM APD dark current data of Fig. 5, when the spatial distribution of dark carrier generation is taken into consideration.

Fig. 8 shows that unlike the avalanche-initiating photoelectrons, which enter the multiplication region at $x = 0$ (the $p+$ side of the multiplication region), the SCM APD dark carriers may be generated uniformly among the gain stages. The dark carriers generated in each individual gain stage, j, initially have too little kinetic energy to impact-ionize and therefore do not multiply within the stage in which they are generated, but ionize with probability P at each of the $J - j$ gain stages they traverse before recombining at the $n+$ contact. The hole carriers drift in the negative x direction, toward the $p+$ contact, ionizing with probability U in each of the $j - 1$ gain stages they traverse. Because of their distributed points of origin, none of the dark carriers experience the full avalanche gain, and hence each dark carrier contributes less gain and gain fluctuation than the photoelectrons.

III. Analytical SCM APD Performance Models Considering Spatial Origin of Ionization Chain

A. Photon-Originated Ionization

The avalanche noise in an APD is generally characterized by the normalized second central moment of the gain random variable for a single input photocarrier,

$$F_e = \langle M^2 \rangle / \langle M \rangle^2. \tag{5}$$

The excess noise is most often found from a measurement of the noise spectral intensity of an APD's photocurrent, using an expression derived from the Burgess-variance theorem [25] and an extension of the Milatz-theorem [26] as

$$F_e = S_I / 2q \langle M \rangle^2 \langle I_p \rangle \tag{6}$$

where $<M>$ is the average avalanche gain measured between the contacts of an APD, and $<I_p>$ is the unmultiplied photocurrent.

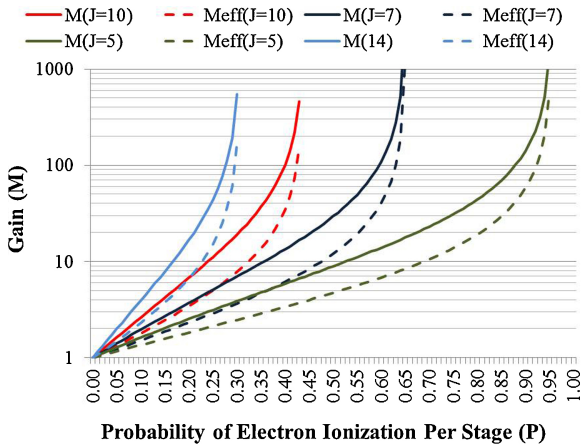

Fig. 9. Modeled primary carrier ($x = 0$ insertion) gain and effective gain (M_{eff}) from dark carrier originating from multi-stage SCM APDs as a function of electron ionization rate per stage, P. The effective gain is calculated (15) by determining the equivalent photocurrent at the $p+$ contact that would equal the multiplied contribution at the device output ($n+$ contact). Also shown is the total gain from all J stages from carriers originating at the $p+$ contact ($x = 0$). Both M and M_{eff} were calculated assuming $k_s = 0.02$.

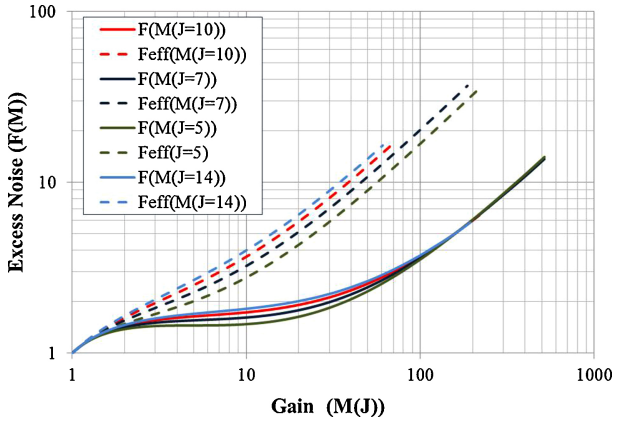

Fig. 10. Modeled effective excess noise (F_{eff}) from the average unmultiplied dark carriers originating in multi- J-stage SCM APDs calculated by (17) as a function of effective gain (M_{eff}) calculated from (15). The effective excess noise calculates the noise required to create the same output variance for input-referred dark carrier contributions. The excess noise (8) from all J stages (F_J) as a function of gain (7) is also shown for both devices. The models assume $k_s = U/P = 0.02$.

Using the single-carrier discrete gain-stage APD model developed by Capasso [10] as modified by VanVliet [13] and improved by Teich [12] to describe dual-carrier multiplication in multiple discrete-stage APDs, we can express the gain measured between the SCM APD contacts as [13]

$$< M_J >= \frac{(1+P)^J (1-k_s)}{(1+k_s P)^{J+1} - k_s (1+P)^{J+1}} = \frac{(1+P)^J (P-U)}{P(1+U)^{J+1} - U(1+P)^{J+1}} \quad (7)$$

where J is the number of gain stages, and $k_s = U/P$. The excess noise factor is given by [12]

$$F_J = 1 + \frac{\left(1 - 1/M_J\right)(1-k_s)}{(2+p(1+k_s))} * \left[-P + 2\frac{(1-k_s P^2)}{(1+k_s P)}\left(\frac{M_J k_s (1+P)}{(1-k_s)} + \frac{1}{1+P}\right)\right]. \quad (8)$$

There currently does not exist a model of the count distribution for two carrier ionization in discrete, multiple gain stage multipliers. For the limit of $k \to 0$, Matsuo et al. [27] derived the gain distribution $p(M)$ for single-carrier discrete-multi-stage APDs in terms of J and P:

$$p_J(M) = (1-P)\, p_{J-1}(M) + P \sum_{k=0}^{M} p_{J-1}(M-k)\, p_{J-1}(k), \quad (9)$$

assuming:

$$M \geq 1,\ J \geq 1;\ p_J(0) = 0,\ J \geq 1;\ \text{and}\ p_o(n) = \delta_{1,n}.$$

The mean of the distribution is given by

$$< M_J >= (1+P)^J, \quad (10)$$

and the variance is

$$\text{var} < M_J >= (1-P)[(1+P)^{2J-1} - (1+P)^{J-1}]. \quad (11)$$

In response to a Poisson number of photocarriers, <a>, at the input, the output counting distribution $q_J(n)$ can be calculated as [27]

$$q_J(n+1) = {<a>}/{(n+1)} \sum_{k=0}^{n} (k+1) q_J(n-k) A_J(k+1), \quad (12)$$

where

$$A_J(k) = (1-P)\, A_{J-1}(k) + P \sum_{l=1}^{k-1} A_{J-1}(k-l)\, A_{m-J}(l), \quad (13)$$

$A_J(0) = 0$ for all J, $A_0(1) = 1$, and $k > 0$.

B. Random Spatial Origination of Dark Ionization Chains

O'Reilly [28] expanded this framework to include analytical models of the gain and excess noise statistics of two-carrier ionization originating from arbitrary discrete locations in a cascaded discrete-gain-stage multiplier.

For the J-stage SCM APD, the unmultiplied dark current induced in the external circuit by the electron-hole pair creation can be expressed as i_j. This local dark current will enter the multiplication process and will experience a random gain m_j, which will induce an output current, φ_j, at the device contacts.

If I_{dark} is the output dark current contribution by all stages measured between the device contacts, then

$$I_{dark} = \sum_{j=1}^{J} \varphi_j, \quad (14)$$

where the effect of dark current generated in the absorption region can be included by starting the summation at $j = 0$. Assuming the dark current components are statistically independent, then

$$< I_{dark} >= \sum_{j=1}^{J} <\varphi_j> = \sum_{j=1}^{J} < I_j >< m_j >. \quad (15)$$

The noise spectral density of I_{dark} can then be expressed as

$$S_J = \sum_{j=1}^{J} S_j = 2q \sum_{j=1}^{J} < I_j > < m_j >^2 F_j, \quad (16)$$

where S_j is the noise spectral density of φ_j and $2q<i_j>$ represents the shot noise density associated with i_j, and F_j is the excess noise factor resulting from the gain at each gain stage.

The number of possible occurrences an electron originating at the j^{th} gain stage can ionize while moving to the $n+$ contact is $J-j$, and the number of possible ionizations the initiating hole can undergo as it drifts to the $p+$ contact is $j-1$. The average gain, $<m_j>$, associated with the electron-hole pair initiating at each stage is thus given by [28]

$$< m_j >= M_J \left(\frac{1+P}{1+U} \right)^{j-J} = M_J (Q)^{j-J}, \quad (17)$$

where $Q = (1+P)/(1+U)$.

The effective excess noise associated with the initiating electron-hole pair at position j is

$$F_j = \frac{\langle m_j^2 \rangle}{\langle m_j \rangle^2}. \quad (18)$$

This can be expressed as [28]

$$F_j = (Q)^{J-j} F_J - \left[2(1-UP)(Q^{J-j}-1) / (1+U)^2 Q \right]. \quad (19)$$

It is useful to treat the unmultiplied primary dark current, $I_d = \sum_{j=1}^{J} i_j$, in a manner similar to the photocurrent generated in the $p+$ region. To allow the primary dark current to be input-referred, an effective gain, M_{eff}, and effective excess noise factor, F_{eff}, can be calculated, which for a photosignal originated in the $p+$ region would result in the same mean and variance signal at the output as the dark current measured between the SCM APD contacts. Assuming equal contribution from each gain stage [28],

$$M_{eff} = \frac{< M_J >}{J} \left(\frac{1-Q^{-J}}{1-Q^{-1}} \right). \quad (20)$$

Plots of M and M_{eff} are shown in Fig. 9, for the case of a 7-stage and a 10-stage SCM APD assuming $k_s = 0.035$. The effective excess noise, F_{eff}, is expressed as [28]

$$F_{eff} = \frac{J\left(Q^2-1\right) Q^J F_J - 2\left\{\left(P-UQ^2\right)(1+U)\right\}\left(Q^{J-1}-1\right)}{Q(Q+1)\left(Q^J-1\right)}. \quad (21)$$

Plots of F_J and F_{eff}, as a function of the hole ionization probability, for the case of a 7-stage and 10-stage SCM APD, assuming $k_s = 0.002$ are shown in Fig. 10.

If we would like to treat the measured primary dark current I_{dark} in a similar manner to photocurrent generated in the $p+$ region, so that when undergoing the full gain of the multiplier the same output dark current I_{dark} is reproduced, then an equivalent dark current, I_{deff}, can be calculated by

$$I_{deff} = < I_{dark} > / M_J. \quad (22)$$

When the average unmultiplied dark current generated in each gain stage is equal,

$$I_{deff} / i_j = \sum_{r=1}^{J} \left[\frac{(1+P)}{(1+U)} \right]^{j-J} = \frac{1 - \left[(1+U)/(1+P) \right]^J}{1 - \left[(1+U)/(1+P) \right]} = \frac{1-Q^J}{1-Q}, \quad (23)$$

the excess noise factor for I_{deff} is expressed as

$$F_{deff} = S_J / (2q I_{deff} M_J^2) = \frac{\sum_{k=1}^{J} F_k Q^{2(k-J)}}{\sum_{k=1}^{J} Q^{(k-J)}}. \quad (24)$$

Using (20)–(24), the photocurrent-gain-compensated dark current data measured for the 10-stage SCM APDs were corrected to better reflect the devices' dark carrier properties. The resulting mean effective gain-compensated dark current data are shown in Fig. 3. Note that the corrected primary dark count levels are higher than those predicted assuming photocurrent gain levels.

The data also suggest that as the bias approaches the breakdown voltage, a secondary signal source, perhaps due to sidewall effects, is likely present, which resulted in an overestimation of the gain at high biases and caused the gain-compensated dark current curves to decrease at the higher biases. In this work, we did not attempt to characterize this secondary signal source further, as it occurred largely outside the operational range of the devices [11].

IV. Numeric Models of Instantaneous Gain and Excess Noise of Randomly Originated Carriers in the SCM APD

The above analytical models are useful for describing the low order statistical characteristics of the SCM APD under pseudo-DC conditions, but they do not provide the instantaneous properties of the device over the times of the impulse response, which are necessary to predict optical pulse detection probabilities [9]. The excess noise and PDF models typically used to quantify APD gain fluctuations assume that the gain is integrated over the entire impulse response curve [11]. However, optical pulses are often shorter than the duration of an APD impulse response, and threshold detection circuits of the high-speed optical receivers often operate on the leading portions of signal pulse. In either of these cases, the optical signals are amplified only by the partial gain of the APD accumulated during the earliest times of the impulse responses. Thus, the signal detection processes cannot be accurately predicted using the analytical DC gain and noise models introduced earlier, which all assume instantaneous amplification at time scales less than the pulse duration.

For real-world applications, accurate prediction of pulse detection efficiency and false alarm rate necessitates knowledge of the instantaneous properties of SCM APD impulse response. The calculation of the instantaneous photocurrent variance requires knowledge of the second moment at each time of the impulse-response function, and the calculation of the integrated photocurrent variance necessitates the autocorrelation function of the optical and dark signals [29], [30].

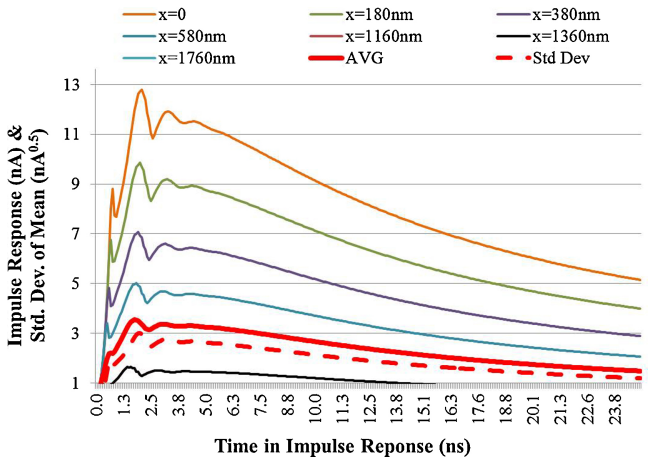

Fig. 11. Numeric model of the impulse current response of an SCM APD operated at a bias for $M = 940$ showing, over $T = 25$ transit times, the induced photocurrent contributions from carriers originating at different locations in the multipliers as a function of avalanche buildup time. The average and standard deviation of the dark carrier contributions are also plotted ($x = 0$ models a photoelectron injected into the multiplier).

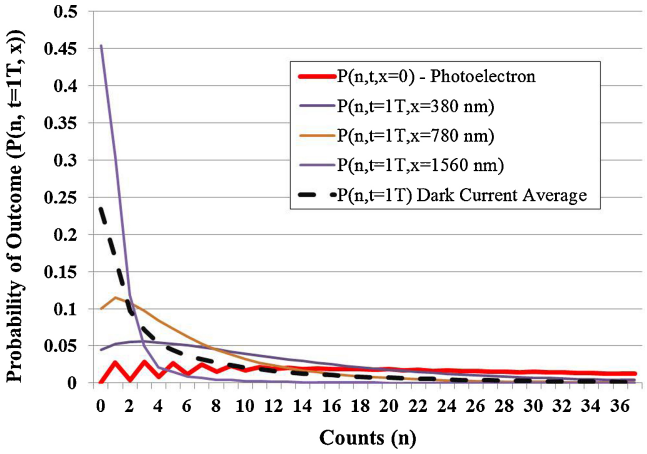

Fig. 12. Output pulse count (n) distribution at $T = 1$ transit times showing the photon-originated $x = 0$, dark $x = 380$-nm (2^{nd} gain stage), dark $x = 960$-nm (5^{th} gain stage), and average-originated count distributions.

The calculation of counting distributions and statistical moments of an APD is often difficult, requiring the use of numerical integration even in simple device structures. Accordingly, to characterize the mean gain and excess noise characteristics of SCM APD photon- and dark-initiated carriers over the times of its impulse response, we developed a numeric model of the SCM APD based on the framework of dead space multiplication theory (DSMT) [7], [31]. The DSMT models include an age-dependent recursive theory for avalanche multiplication that facilitates the calculation of the mean, variance, and excess noise factors during the times of the impulse response.

To accurately model the SCM APD, we modified the DSMT models to allow for the spatial distribution of ionization events for arbitrary heterojunction multiplication regions to be calculated. To accommodate carrier phonon scattering in low field regions of the SCM APD multiplication region, "scattering aware" ionization coefficients were created, which along with the calculated electron- and hole- dead-space coefficients, were used in expressions that generate the PDF of the distance to the first occurrence of impact ionization [8].

Using the approach described by Hayat and Saleh [32], recursive equations were solved to yield the moment generating function (MGF) of the stochastic quantities of electrons and holes at time, t, which originated at location, x. The recursive equations allowed us to determine the number of impact ionization events triggered by electrons and holes in an arbitrary sub-region of the multiplication region.

Fig. 2 plots the numeric DSMT simulation of the spatial occurrence of hole and electron ionization events in a 10-gain-stage SCM APD against the multiplication layer's spatially varying electric field profile, when biased for an average DC gain of $M_{DC} = 940$.

This new technique also facilitated the computation of the PDF of the impulse response function at any arbitrary time over a specified time interval. From these, the temporally resolved MGF of the impulse response, $I(t)$, was derived, from which the probability mass function was obtained via a simple Fourier-inversion applied to the MGF.

To investigate the influence of SCM APD dark carriers on receiver performance, the instantaneous properties of SCM APD impulse response to photon-initiated carriers generated at $x = 0$, and dark-initiated avalanche events originating at random discrete locations in the multiplier, were determined from analysis of carrier motion in the multiplication region over the times of the impulse response. By analyzing the temporal dynamics of the ionization chains and adding the current contributions from all the offspring electrons and holes that were traveling in the multiplication region at all times, the instantaneous properties of the impulse response were calculated [33].

Fig. 11 shows the numerically modeled mean impulse response curves for photon-initiated avalanche events originating at $x = 0$ and dark-initiated avalanche events originating from various gain stage locations. The impulse response curves plot, as a function of transit times, the mean current induced in the junction by impact ionization of dark carriers originated at the various spatial locations. Also plotted are the average and standard deviation of the impulse response originating from dark events generated uniformly among the 10 gain stages. The numeric data confirm that the dark carriers do not experience full gain, as the average dark current induced in the circuit is significantly lower in magnitude than the photoelectron-induced current. For example, at the peaks of the photon- and dark-originating impulse response curves, both which occur at about $T = 1$ transit times, the mean current induced by the average of the dark carriers is 33 nA, with a standard deviation of 0.209 nA, whereas the mean photon-initiated carrier generates 187 nA, with a standard deviation of 0.692 nA. The SCM APD multiplication region is approximately 2-μm long, and for $v = 5*10^4$ cm/s the transit time, T, is approximately 276 ps.

Fig. 12 shows output count distributions at $T = 1$ transit times after carrier creation for various carrier origination locations, $P(n,T = 1,x)$, where n is the count outcome, and x is the spatial location of the ionization chain's origin. The

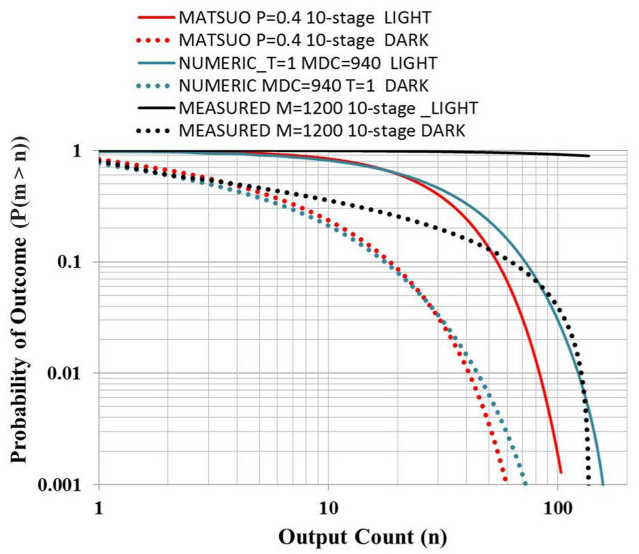

Fig. 13. Probability of detection for the DSMT numeric model at $T = 1$ ($M_{DC} = 940$), assuming single photoelectron input; the Matsuo analytical model (9) assuming pseudo-DC conditions and no hole feedback (9; $P_e = 0.4$, $k_s = 0.035$); and measured SCM APD data ($M_{DC} = 1\,200$).

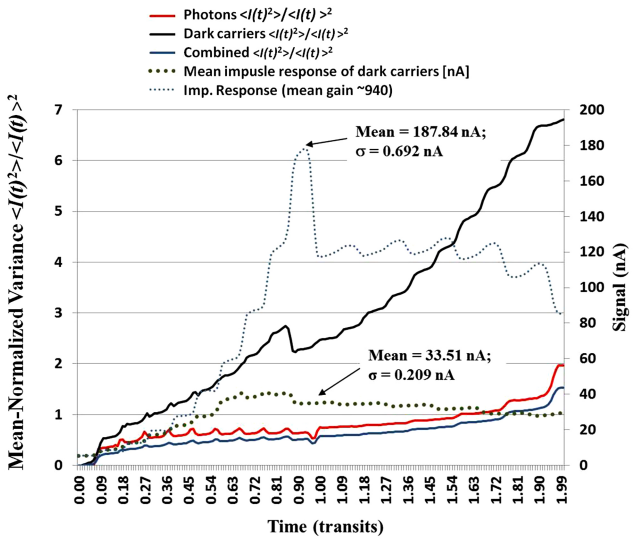

Fig. 14. Instantaneous excess noise modeled as the gain-normalized mean current as a function of transit time. Shown are three cases: 1) a photon-originating carrier; 2) an average dark-originating carrier; and 3) a combined signal from both photons and dark events. Shown for reference is the impulse response curve for the photon-originating ($x = 0$) signal. In this model, the SCM APD was biased for $<M_{DC}> = 940$ and the total cumulative excess noise was $F(M_{DC}) = 0.036$. The mean and variance are shown for $t = 1T$ transit times.

$P(n,1T,0\text{-nm})$ count distributions show a nearly uniform distribution, whereas $P(n,1T,380\text{-nm})$, $P(n,1T,750\text{-nm})$, $P(n,1T,1560\text{-nm})$, and the average distribution from dark carriers originating randomly in the gain stage distributions $P(n,1T, <x>)$ are skewed toward $n = 0$. The count distributions clearly have a lower mean gain contribution from ionization chains originating from dark carriers generated in the later gain stages.

Fig. 13 shows the cumulative PDFs of photon- and dark-originating avalanche events for the DSMT numeric model of an $M_{DC} = 940$ biased SCM APD at $T = 1$ transit times. The numeric models are plotted alongside the analytically modeled PDFs calculated from (9), parameterized by $J = 10$ and $P = 0.4$. Although (9) assumes single-carrier ionization and instantaneous gain (pseudo-DC conditions), it is useful in modeling the impulse response at $t = 1T$ transit times, as at these times, the SCM APD impulse response is dominated by electron ionization events [8]. As expected, (9) underestimates the higher count probabilities of the numeric model, which includes some hole ionization feedback. Measured data for a 50-micrometer diameter SCM APD, acquired using a 2.1 GHz amplifier, are also shown, albeit biased for higher gain ($<M> = 1200$). In the data shown in Fig. 13, the amplifier noise is deconvolved from the data. All of the data sets clearly show SCM APD ability to discriminate single photon events from dark events.

Using the numerically derived photon- and dark-originating PDFs over all of the times of the impulse response, carrier-induced impulse response currents were generated for the case of: 1) photon-initiated signal current; 2) average dark-initiated signal current; and 3) the combined signal from photon- and dark-originating carrier contributions, where the mean impulse response of the dark carriers, $\overline{I_{dark}}(t)$, was calculated from the dark current generation rates calculated by (4) and shown in Fig. 8, assuming a 100-micrometer diameter SCM APD. The instantaneous gain-normalized variance, ($<I(t)^2>/<I(t)>^2$), for each case, is plotted in Fig. 14. The large variance of the dark-originating current compared to the photon-originating current is evident, and due to the difference in mean gain between the photon-initiated and dark-initiated signal currents, the ability to discriminate photon events from dark events over the entire $t = 2T$ transit time period is obvious.

For both photon- and dark-initiated impulse responses, the cumulative excess noise from the partial gain can be estimated by $\left(\int_0^t \sqrt{m(k)}\right)^2 / \left(\int_0^t m_t\right)^2$. The exact expression of the second moment of the cumulative impulse response, namely $<I(t)^2>$ is the double integral of the autocorrelation function of the instantaneous impulse response, $<I(g)I(s)>$, with each of the variables g and s ranging from 0 to t. For the case when only noise is present, the mean and the variance are given by [34]

$$\mu_0 = \varphi \int_0^{Tb} \int_0^t \left\langle \overline{I_p}(t-\xi) \right\rangle d\xi dt \tag{25}$$

and

$$\sigma_0^2 = \varphi \int_0^{Tb} \int_0^{Tb} \int_0^{g \wedge s} \overline{R_{Ip}}(g-\xi, s-\xi) d\xi dg ds, \tag{26}$$

where $\overline{R_{Ip}}(t_1, t_2)$ is the autocorrelation function of the dark carriers averaged over the multiplication region, and φ is the dark-carrier generation rate.

V. Effects of Dark Carrier Contributions on Receiver Performance

Using the cumulative instantaneous gain and excess noise properties of the photon- and dark-originated carriers

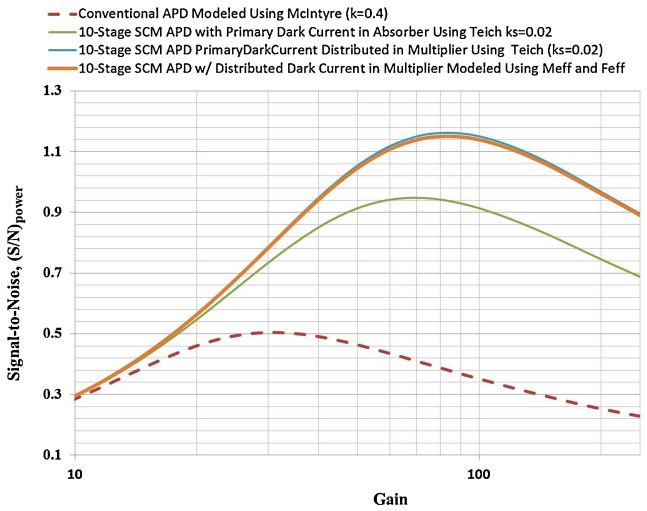

Fig. 15. Photoreceiver signal to noise S/N_{power} from (24) for: 1) a conventional InGaAs/InP SACM APD, modeled using McIntyre equation ($k = 0.4$); 2) a 10-stage SACM APD with dominant dark current from absorber, modeled assuming equivalent excess noise and gain for photon- and input- referred dark current using (8; $k_s = 0.02$); 3) the 10-stage SACM APD with dark current from multiplier dominating, modeled without reference to spatial origin (8; $k_s = 0.02$); and 4) the 10-stage SACM APD with dark current from multiplier dominating, modeled correcting for spatial origin using M_{eff} and F_{eff}.

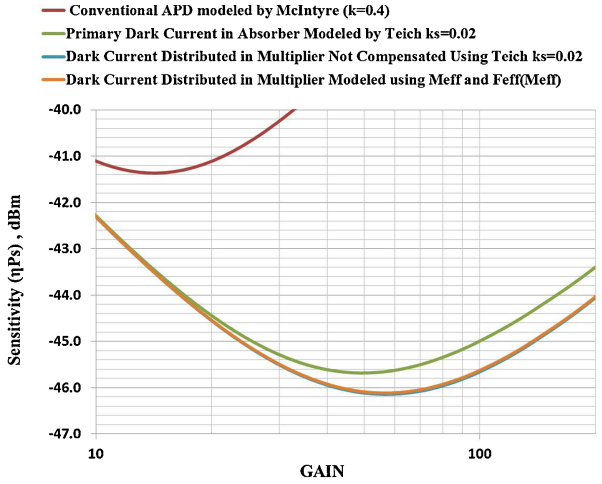

Fig. 16. Photoreceiver sensitivity (25) modeled for: 1) a conventional InGaAs/InP SACM APD, modeled using McIntyre equation ($k = 0.4$); 2) a 10-stage SACM APD with dominant dark current from absorber, modeled assuming equivalent excess noise and gain for photon- and input- referred dark current using (8; $k_s = 0.02$); 3) the 10-stage SACM APD with dark current from multiplier dominating, modeled without reference to spatial origin (8; $k_s = 0.02$); and 4) the 10-stage SACM APD with dark current from multiplier dominating, modeled correcting for spatial origin using M_{eff} and F_{eff}.

generated in the SCM APD, it is possible to predict receiver performance. One of the key engineering figures of merit used in describing the operation of a photodetector is its signal-to-noise power ratio, $(S/N)_{power}$, which is useful in characterizing the capability of the device to distinguish a small input signal from inherent noise sources and is of great importance in describing device performance. $(S/N)_{power}$ is mathematically determined by

$$\left(\frac{S}{N}\right)_{power} = \frac{1/2\left(I_p\right)^2}{2qB\left(I_p F_J + I_{deff} F_{deff}\right) + {4kTB}/{\left(R_{eq} < M_J >^2\right)}} \tag{27}$$

where I_p is the steady-state photocurrent, given by $I_p = q\eta P_{opt}/h\nu$, where η is the device quantum efficiency, q is the capacitance of an electron, B is the the bandwidth, and $4kTB/R_{eq}$ is the noise contribution from the amplifier using the noise equivalent resistance, R_{eq}.

Although a complete analytical characterization of the SCM APD in terms of the gain MGFs is not currently available, the sensitivity of an APD receiver, based on the first and second order moments, can be approximated by [35]

$$\eta P_s = \frac{hc}{q\lambda} Q_o \left(\frac{\langle i_n^2 \rangle^{1/2}}{M_J} + qBQ_o F(M_J) I_1 \right), \tag{28}$$

where P_s is the mean optical power incident on the device, c is the velocity of light, I_1 and I_2 are the Personick integrals [35], Q_o is related to the bit-error rate (BER) ($Q_o = 6$ for BER $= 10^{-9}$) [35], and the noise current, i_n, composed of the amplifier circuit noise, i_a, and the thermal dark current noise, i_{th}, is given by

$$i_n = (i_a^2 + i_{th}^2)^{1/2} = \left[i_a^2 + 2qI_{deff} M_J^2 F_{deff}(M_J) I_2 B \right]^{1/2}. \tag{29}$$

The $(S/N)_{power}$ and sensitivity of a 10-stage SCM APD receiver are plotted in Fig. 15 and Fig. 16, respectively, assuming a 2.1 GHz transimpedance amplifier with 275 mA root mean square (RMS) noise. We considered the cases where dark current originated in either the absorber or the multiplier: 1 nA measured at unity gain for either case.

Four cases were considered: 1) a conventional bulk-semiconductor multiplier APD described by the McIntyre-distribution [11] parameterized by $k = 0.4$; 2) a 10-stage SCM APD with dark current originating in the absorber, with equal treatment of the photon- and dark-originating carrier excess noise modeled using a Van Vliet/Teich model (8; $k_s = 0.02$); 3) an SCM APD, wherein the dark current originates uniformly in the high field regions of the multiplication region, but is input-referred without regard to its origin, i.e., $I_{dark}/<M_J>$, using (8; $k_s = 0.02$); and 4) an SCM APD, wherein the dark current originates in the multiplier, and proper treatment of the gain and excess noise is performed using (18) and (19). The data show that the SCM APD is capable of considerably better $(S/N)_{power}$ performance than a conventional APD. The data also show the importance of accurately determining the spatial origin of the dominant dark current source, when modeling SCM APD performance.

VI. Summary and Conclusion

The DSMT numeric models used to characterize current induced in the external receiver circuits by photon- and dark-originating ionization carriers in the multiplication region of the SCM APD demonstrate the capability to discriminate photon counts from dark counts. This is particularly significant for wide bandgap $Al_yGa_xIn_{1-x-y}As$ absorption layer SCM APDs and cold-temperature operation of SCM APDs, whereby thermally generated dark current is insignificant compared to the tunneling dark current originating in the high field regions of the multiplier.

We have shown that analytical models of cascaded, discrete-gain-stage devices are useful in describing the SCM APD behavior, allowing for accurate treatment of measured data under pseudo-DC conditions. Both the numeric and analytical models show the statistical differences in the optical and dark signals from the SCM APD and help to elucidate the differences between the SCM APD and a conventional bulk-semiconductor multiplier. The data show both the performance benefits of SCM APDs over conventional bulk-InP multiplier APDs and the errors that result when the origin of the dark current is not taken into account during measurements, data treatment, and performance modeling.

Unlike the analytical models, the DSMT numeric model does not involve any fitting parameters to the data; it only uses universal parameters for non-localized ionization coefficients, material ionization threshold energies, and simple scattering rules.

Uniquely, the DSMT numeric models of the SCM APD provide the time-resolved PDF descriptions of the photon- and dark- originating carriers necessary for determining the probability of single photon detection and for generating receiver operation characteristic (ROC) curves.

REFERENCES

[1] G. Agrawal, *Fiber-Optic Communication Systems*. New York, NY, USA: Wiley, 2002.

[2] B. E. A. Saleh and M. C. Teich, *Fundamentals of Photonics*. NewYork, NY, USA: Wiley, 2007.

[3] G. E. Stillman, V. M. Robbins, and N. Tabatabaie, "III-V compound semiconductor devices: Optical detectors," *IEEE Trans. Electron Devices*, vol. 31, no. 11, pp. 1643–1655, Nov. 1984.

[4] Capasso, "Chapter 1: Physics of avalanche photodiodes," in *Semiconductors and Semimetals*, R. K. Willardson and A. C. Beer, Series Eds., vol. 22, part D, *Lightwave Communications Technology—Photodetectors*, W. T. Tsang, Ed. New York, NY, USA: Academic, 1985, pp. 1–172.

[5] R. Chin, N. Holonyak, G. E. Stillman, J. Y. Tang, and K. Hess, "Impact ionization in multilayered heterojunction structures," *Electron Lett.*, vol. 16, pp. 467–469, Jun. 1980.

[6] F. Capasso, W. T. Tsang, A. L. Hutchinson, and G. F. Williams, "Enhancement of electron-impact ionization in a super-lattice: A new avalanche photo-diode with a large ionization ratio," *Appl. Phys. Lett.*, vol. 40, pp. 38–40, Jan. 1982.

[7] G. M. Williams, M. A. Compton, and A. S. Huntington "Single-photon-sensitive linear-mode APD Ladar receiver developments," in *Proc. SPIE Laser Radar Technol. Appl.* vol. 13, Apr. 2008, p. 6950.

[8] G. M. Williams, D. A Ramirez, M. M. Hayat, and A. S. Huntington, "Time resolved gain and excess noise properties of InGaAs/InAlAs avalanche photodiodes with cascaded discrete gain layer multiplication regions," *J. Appl. Phys.*, vol. 113, p. 093705, Mar. 2013.

[9] G. M. Williams, M. Compton, D. A. Ramirez, M. M. Hayat, and A. S. Huntington, "Multi-gain-stage InGaAs avalanche photodiode with enhanced gain and reduced excess noise," *IEEE J. Electron. Devices*, vol. 1, no. 2, pp. 54–65, Feb. 2013.

[10] F. Capasso, W. T. Tsang, and G. F. Williams, "Staircase solid-state photomultipliers and avalanche photodiodes with enhanced ionization rates ratio," *IEEE. Trans. Electron. Devices*, vol. 30, no. 4, pp. 381–390, Apr. 1983.

[11] R. J. McIntyre, "Multiplication noise in uniform avalanche diodes," *IEEE Trans. Electron. Devices*, vol. 13, no. 1, pp. 164–168, Jan. 1966.

[12] M. C. Teich, K. Matsuo, and B. E. A. Saleh, "Excess noise factors for conventional and superlattice avalanche photodiodes and photomultiplier tubes," *IEEE J. Quantum Electron*, vol. 22, no. 8, pp. 1184–1193, Aug. 1986.

[13] K. M. van Vliet, A. Friedmann, and L. M. Rucker, "Theory of carrier multiplication and noise in avalanche devices—Part II: Two-carrier processes," *IEEE Trans. Electron Devices*, vol. 26, no. 5, pp. 752–764, May 1979.

[14] S. R. Forrest, "Performance of InxGa1-xAsyP1-yphotodiodes with dark current limited by diffusion, generation recombination, and tunnelling," *IEEE J. Quantum Electron.*, vol. 17, no. 2, pp. 217–226, Feb. 1981.

[15] M. A. Itzler, X. Jiang, R. Ben-Michael, K. Slomkowski, M. A. Krainak, S. Wu, and X. Sun, "InGaAsP avalanche photodetectors for non-gated 1.06 micron photon-counting receivers" in *Enabling Photonics Technologies for Defense, Security, and Aerospace Applications III*, M. J. Hayduk, A. R. Pirich, P. J. Delfyett, Jr. *et al.*, Eds., *Proc. SPIE*, vol. 6572, Apr. 2007.

[16] R. N. Hall, "Electron-hole recombination in germanium," *Phys. Rev.*, vol. 87, no. 2, p. 387, Jul. 1952.

[17] S. Paul, J. B. Roy, and P. K. Basu, "Empirical expressions for the alloy composition and temperature dependence of the band gap and intrinsic carrier density in GaxIn1-xAs," *J. Appl. Phys.*, vol. 69, pp. 827–829, Jan. 1991.

[18] D. Olego, T. Y. Chang, E. Silberg, E. A. Caridi, and A. Pinczuk, "Compositional dependence of band-gap energy and conduction-band effective mass of In1-x-yGaxAlyAs lattice matched to InP," *Appl. Phys. Lett.*, vol. 41, pp. 476–478, Sep. 1982.

[19] J. P. Donnelly, E. K. Duerr, K. A. McIntosh *et al.*, "Design considerations for 1.06-μm InGaAsP-InP Geiger-mode avalanche photodiodes," *IEEE J. Quantum Electron.*, vol. 42, no. 8, pp. 797–809, Aug. 2006.

[20] J. L. Moll, *Physics of Semiconductors*. New York, NY, USA: McGraw-Hill, 1964, p. 253.

[21] D. W. Winston and D. Wells, "Physical simulation of optoelectronic semiconductor devices," Ph.D. thesis, Dept. Electr. Eng. Comput. Eng., Univ. Colorado, Boulder, CO, USA, 1996.

[22] D. Biswas, A. Chin, J. Pamulapati, and P. Bhattacharya, "Traps in molecular beam epitaxial In0.53(GaxAl1-x)0.47As/InP," *J. Appl. Phys.*, vol. 67, no. 5, Mar. 1990.

[23] J. C. Campbell, "Low-noise large-area avalanche photodiodes," Microelectronics Res. Center, Univ. Tex. Austin, TX, USA, AFOSR/NE Final Rep. F49620-03-1-0001, Mar. 2004.

[24] G. B. Stringfellow, *Organometallic Vapor-Phase Epitaxy: Theory and Practice*, 2nd ed. San Diego, CA, USA: Academic, 1999, p. 407.

[25] K. Matsuo, K. B. Saleh, and M. Teich, "Excess noise factors for conventional and superlattice avalanche photodiodes and photomultiplier tubes,"*IEEE J. Quantum Electron.*, vol. 22, no. 8, pp. 1184–1193, Aug. 1986.

[26] A. van der Ziel, *Noise in Solid State Devices and Circuits*. New York, NY, USA: Wiley, 1986, pp. 14–18.

[27] K. Matsuo, M. C. Teich, and B. E. A. Saleh, "Noise properties and time response of the staircase avalanche photodiode," *IEEE Trans. Electron. Devices*, vol. 32, no. 12, pp. 2615–2623, Dec. 1985.

[28] J. J. O'Reilly and R. S. Fyath, "Analysis of the influence of dark current on the performance of optical receivers employing superlattice APDs," in *IEEE Proc. J. Optoelectron.*, vol. 135, pp. 109–118, Feb. 1988.

[29] M. M. Hayat, B. E. A. Saleh, and J. A. Gubner, "Bit-error rates for optical receivers using avalanche photodiodes with dead space," *IEEE Trans. Commun.*, vol. 43, no. 1, pp. 99–106, Jan. 1995.

[30] M. M. Hayat, O. Kwon, Y. Pan, P. Sotirelis, J. C. Campbell, B. E. A. Saleh, and M. C. Teich, "Gain-bandwidth characteristics of thin avalanche photodiodes," *IEEE Trans. Electron. Devices*, vol. 49, no. 5, pp. 770–781, May 2002.

[31] D. A. Ramirez, A. S. Huntington, G. M. Williams, and M. M. Hayat, "Non-local model for the spatial distribution of impact ionization events in avalanche photodiodes," *Appl. Phys. Lett.*, 2013, submitted for publication.

[32] M. M. Hayat and B. E. A. Saleh, "Statistical properties of the impulse response function of double-carrier multiplication avalanche photodiodes including the effect of dead space," *J. Lightw. Technol.,* vol. 10, no. 10, pp. 1415–1425, Oct. 1992.

[33] M. M. Hayat and G. Dong, "A new approach for computing the bandwidth statistics of avalanche photodiodes," *IEEE Trans. Electron. Devices*, vol. 47, no. 6, pp. 1273–1279, Jun. 2000.

[34] P. Sun, M. M. Hayat, B. E. A. Saleh, and M. C. Teich, "Statistical correlation of gain and buildup time in APDs and its effects on receiver performance," *J Lightw. Technol*, vol. 24, no. 2, pp. 755–768, Feb. 2006.

[35] R. G. Smith and S. D. Personick "Chapter 4: Receiver design for optical fiber communication systems," in *Semiconductor Devices for Optical Communication* (Topics in Applied Physics, vol. 39), H. Kressel, Ed. Princeton, NJ, USA: Springer, 1982, pp. 89–160.

George Williams is the President of Voxtel, Inc., and oversees Voxtel's R&D and commercial product sales. Mr. Williams also contributes technically in the engineering of X-ray, UV, visible, NIR, infrared, night vision, and multi-spectral EO systems. He has been involved in researching, designing, and manufacturing image sensors, imaging systems, and image processing algorithms for over 25 years. His specific technical expertise includes active and passive electro-optical system design and modeling, as well as silicon CCD and CMOS, InGaAs, image intensified detector, and HgCdTe detector design and manufacturing. He also takes an active lead in nanocrystal-based photovoltaics, thermoelectric coolers, and upconverting and downconverting nanocrystal film device development. Previously, as Executive VP and General Manager of PixelVision, Inc. and its sister company, SITe, Inc.,

Mr. Williams managed the teams that designed, manufactured, and delivered CCD technology to a variety of commercial and important government programs, including imagers for the Hubble Space Telescope SITS and Advanced Camera, SOHO, as well as other important NASA (Space Shuttle, Chandra, etc.) and DoD missions. While at ITT Night Vision, he developed considerable experience in image-intensified night vision goggles (NVGs) and infrared detector design and development, and led the commercialization of the night vision technology in the NightMariner and NightEnforcer product lines. Mr. Williams holds a DoDTop Secret security clearance.

David A. Ramirez is a Research Scientist at SKINfrared LLC. He received his B.S. and M.Sc. in Electrical Engineering from the University of Concepción, Chile, in 2002 and 2005, respectively. In 2012, he graduated with a Ph.D. in Electrical Engineering from the University of New Mexico. His research interests include the design and fabrication of infrared photodetectors, numerical modeling of semiconductor devices, and scientific computing with Python. In January 2012, Dr. Ramirez was awarded a postdoctoral fellowship by the New Mexico Cancer Nanoscience and Microsystems Training Center (CNTC) to carry out cancer research. Since then, Dr. Ramirez has been collaborating with the multidisciplinary group at SKINfrared LLC that is focused on skin cancer research. At SKINfrared LLC, Dr. Ramirez is involved with the development of an Advanced Longwave Infrared-imaging and Analysis System (ALIAS), fabrication of next generation infrared devices, and the numerical modeling of semiconductor devices.

Majeed M. Hayat was born in Kuwait in 1963. He received his Bachelor of Science (*summa cum laude*) in Electrical Engineering from the University of the Pacific, Stockton, CA, in 1985. He received the M.S. and the Ph.D. degrees in Electrical and Computer Engineering from the University of Wisconsin-Madison in 1988 and 1992, respectively. He is currently a Professor of Electrical and Computer Engineering, Associate Director of the Center for High Technology Materials, and General Chair of the Optical Science and Engineering Program at the University of New Mexico. Dr. Hayat's research activities cover a broad range of topics including avalanche photodiodes, signal and image processing, algorithms for spectral and radar sensing and imaging, optical communication, networked computing, and modeling interdependent networks with applications to smart grids. Dr. Hayat was Associate Editor of Optics Express from 2004 to 2009 and he is currently the Chair of the topical committee of Photodetctors, Sensors, Systems and Imaging within the IEEE Photonics Society. He was a recipient of the National Science Foundation Early Faculty Career Award (1998) and the Chief Scientist Award for Excellence (2006) from the National Consortium for MASINT Research of the Defense Intelligence Agency. Dr. Hayat has authored or co-authored over 82 peer-reviewed journal articles (H-Index = 27) and has six issued patents, three of which have been licensed. Dr. Hayat is a Fellow of SPIE and OSA.

Andrew S. Huntington manages Voxtel's Detector Development Group and is responsible for Voxtel's advanced development efforts relating to semiconductor devices, material growth, device modeling, and detector design and development efforts. He invented and patented Voxtel's advanced high-gain, low-excess-noise SCM-APD technologies, and has supported this important device's development through Monte Carlo modeling and experimental extraction of the material's properties. He has also managed the development of Voxtel's array process and APD-based commercial products. The detector projects Dr. Huntington has conducted include Geiger- and linear-mode SOICMOS and InGaAs-based APDs for the NIR;HgCdTe APDs for the SWIR, MWIR, and LWIR; and silicon-based linear APDs for visible and X-ray applications. He has a number of publications detailing this work. Prior to joining Voxtel, Dr. Huntington performed his doctoral studies in materials at the University of California, Santa Barbara (L. Coldren Group), where his dissertation work included development of low-noise and broad-area InGaAs/InAlAs APDs. That work was conducted in collaboration with Professor Joe Campbell of the University of Texas, Austin, who is widely recognized as a leader in the field. Conducting this work, Dr. Huntington developed his expertise in the production of APD wafers by molecular beam epitaxy, with particular emphasis on understanding the relationship between growth conditions, material quality, and device performance. Dr. Huntington is a US citizen and holds a DoD Secret security clearance.